Independent Actuation of Two-Tailed Microrobots

Islam S. M. Khalil, *Member, IEEE*, Ahmet Fatih Tabak, *Member, IEEE*, Youssef Hamed, Mohamed Tawakol, Anke Klingner, Nesrine El Gohary, Boris Mizaikoff, and Metin Sitti, *Fellow, IEEE*

***Abstract*—A soft two-tailed microrobot in low Reynolds number fluids does not achieve forward locomotion by identical tails regardless to its wiggling frequency. If the tails are nonidentical, zero forward locomotion is also observed at specific oscillation frequencies (which we refer to as the reversal frequencies), as the propulsive forces imparted to the fluid by each tail are almost equal in magnitude and opposite in direction. We find distinct reversal frequencies for the two-tailed microrobots based on their tail length ratio. At these frequencies, the microrobot achieves negligible net displacement under the influence of a periodic magnetic field. This observation allows us to fabricate groups of microrobots with tail length ratio of 1.24 ± 0.11, 1.48 ± 0.08, and 1.71 ± 0.09. We demonstrate selective actuation of microrobots based on prior characterization of their reversal frequencies. We also implement simultaneous flagellar propulsion of two microrobots and show that they can be controlled to swim along the same direction and opposite to each other using common periodic magnetic fields. In addition, independent motion control of two microrobots is achieved toward two different reference positions with average steady-state error of 110.1 ± 91.8 μm and 146.9 ± 105.9 μm.**

***Index Terms*—Beaded fibers, flagellar propulsion, low Reynolds numbers, magnetic, soft microrobot, two-tailed.**

I. Introduction

LOCOMOTION of microrobots in low-Reynolds numbers ($R_e \sim 10^{-5}$) using planar wave propagation has long been proposed to break the constraints of Purcell's scallop theorem [1]. One approach to the actuation of these microrobots is through the action of an oscillating magnetic field [2]–[12]. This field is used for the actuation and directional control. Actuation is achieved by applying uniform fields with a periodic component, whereas directional control is accomplished by directing these fields towards a desired direction of motion. This approach has been implemented and proven to be effective as it depends on relatively weak magnetic field for actuation and control. However, the dual function of the magnetic field to actuate and control, does not allow independent control of multiple microrobots. Donald *et al.* [13] have designed heterogeneous microelectromechanical systems (MEMS) microrobots. These microrobots are classified based on the design of their steering arm actuator that enables independent maneuvering during parallel operations and microassembly. Floyd *et al.* [14] and Diller *et al.* [15], [16] have also achieved motion differentiation through heterogeneous microrobot designs to enable distinct response of the microrobot to the common dynamic driving magnetic fields in two- and three-dimensional spaces, respectively. It has also been demonstrated by Kratochvil *et al.* that magnetic microrobots have the capability to achieve decoupled motion under the influence of a driving magnetic field owing to their different resonant frequencies [17]. Mahoney *et al.* have studied the behaviour of rotating magnetic microrobots above their step-out frequency to achieve microrobot differentiation and independent control [18]. Wong *et al.* have demonstrated independent manipulation of multiple magnets at macro scale and in one-dimensional space through the spatial non-uniformities in the magnetic field [19]. Cappelleri *et al.* have also proposed the utilization of a fine grid of in-plane MEMS-fabricated micro coils to achieve independent control of multiple magnetic microrobots [20]. In this work, we demonstrate the capability of two-tailed microrobots [see Fig. 1(a)] with different tail length ratio to move independently under the influence of a common driving magnetic field. The design of the microrobots enables simultaneous generation of two opposite propulsive forces imparted to the fluid by each tail. First, we model the microrobots based on the resistive-force theory (RFT) and find a relation between the reversal frequency and the tail length ratio. Second, we achieve independent actuation of microrobots using a common driving magnetic field based on their characterized reversal frequencies. We also demonstrate the ability of these microrobots to swim controllably towards different reference positions.

The remainder of the paper is organized as follows: Section II provides modeling of the two-tailed microrobots and simulation of their response. Experimental characterization of the reversal frequencies is conducted based on the frequency response of microrobots with different tail length ratio in Section III. Independent actuation and motion control of the microrobots is demonstrated in Section IV. Finally, Section V concludes and provides directions for future work.

II. Modeling of Two-Tailed Soft Microrobots

We consider a spheroidal head with an average magnetic moment $\mathbf{m}$, coinciding with its major axis. The head is rigidly

Manuscript received September 10, 2017; accepted January 28, 2018. Date of publication February 5, 2018; date of current version February 27, 2018. This letter was recommended for publication by Associate Editor D. Cappelleri and Editor Y. Sun upon evaluation of the reviewers' comments. This work was supported by in part by the DAAD-BMBF funding project and in part by the Science and Technology Development Fund in Egypt (No. 23016). *(Corresponding author: Islam S. M. Khalil.)*

I. S. M. Khalil, Y. Hamed, M. Tawakol, A. Klingner, and N. El Gohary are with the German University in Cairo, New Cairo 11432, Egypt (e-mail: islam.shoukry@guc.edu.eg; Youssef.sabry@student.guc.edu.eg; mohamed.tawakol@student.guc.edu.eg; anke.klingner@guc.edu.eg; nesrine.elgohary@guc.edu.eg).

A. F. Tabak and M. Sitti are with the Department of Physical Intelligence, Max Planck Institute for Intelligent Systems, Stuttgart 70569, Germany (e-mail: tabak@sabanciuniv.edu; sitti@is.mpg.de).

B. Mizaikoff is with the Institute of Analytical and Bioanalytical Chemistry, Ulm University, Ulm 89081, Germany (e-mail: boris.mizaikoff@uni-ulm.de).

Digital Object Identifier 10.1109/LRA.2018.2801793

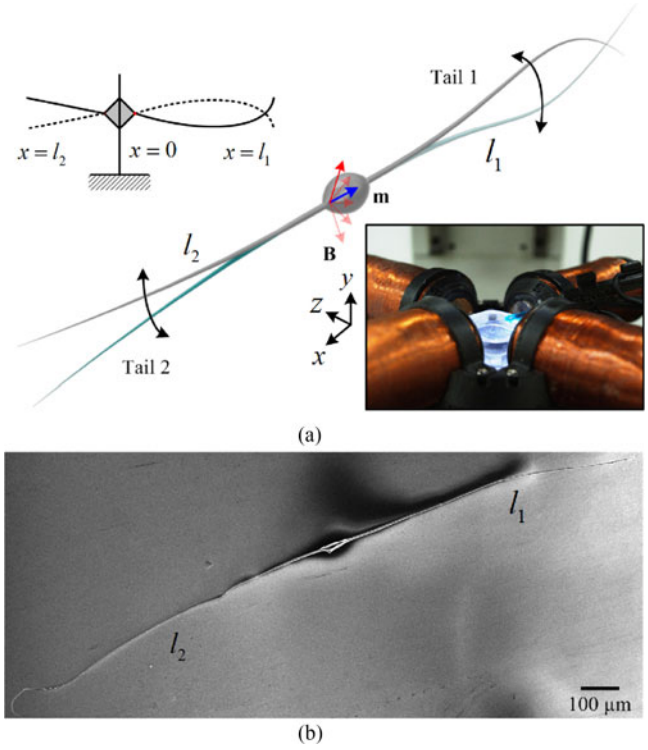

Fig. 1. Soft two-tailed microrobots possess reversal frequencies that enable selective actuation based on their tail length ratio. (a) A schematic representation of the microrobot indicates wave propagation along each tail. The microrobot consists of an elliptical head with magnetic particles embedded within its polymer matrix, and two flexible tails. The particles provide magnetization $\mathbf{m}$ and enable directional control under the influence of a periodic magnetic field $\mathbf{B}$. The magnetic field is provided using an electromagnetic system with orthogonal configuration (inset). Non-identical tails impart unequal propulsive forces to the fluid along opposite directions. The tail length ratio of the microrobot determines its reversal frequency at which negligible net displacement is achieved. (b) A scanning electron microscopy image shows a microrobot with tail length ratio of 1.13. This microrobot achieves negligible displacement regardless to the actuation frequency.

attached at its ends to two flexible tails of length l_1 and l_2, and elasticity E [21], as shown in Fig. 1(b). The two-tailed microrobots are fabricated in a single fabrication step by electrospinning a solution of polystyrene in dimethylformamide [22]. This fabrication process provides continuous beaded fiber. Therefore, the length of the tails can be adjusted to obtain several groups of microrobots with a specific tail length ratio. Magnetic particles are added into the polymer matrix to provide magnetization and enable directional control using magnetic field. The resulting two-tailed microrobot is immersed in a medium characterized by low Reynolds number hydrodynamics, and is driven using periodic magnetic field $\mathbf{B}$. This field is generated using an orthogonal configuration of four electromagnetic coils (see Fig. 1). To calculate the drag force and torque that the microrobot imparts to the fluid, we calculate the resistance matrix $\mathbf{Z}_{\mathrm{r}} = \mathbf{Z}_{\mathrm{h}} + \mathbf{Z}_{\mathrm{t}_1} + \mathbf{Z}_{\mathrm{t}_2}$, where $\mathbf{Z}_{\mathrm{h}}$, $\mathbf{Z}_{\mathrm{t}_1}$, and $\mathbf{Z}_{\mathrm{t}_1}$ are the resistance matrix of the head, first tail, and second tail, respectively. $\mathbf{Z}_{\mathrm{h}}$ is given by

$$\mathbf{Z}_{\mathrm{h}} = \begin{pmatrix} \mathbf{D}_{\mathrm{tran}} & -\mathbf{D}_{\mathrm{tran}}\mathbf{S}_{\mathrm{b}} \\ \mathbf{S}_{\mathrm{b}}\mathbf{D}_{\mathrm{tran}} & \mathbf{D}_{\mathrm{rot}} \end{pmatrix}, \tag{1}$$

where $\mathbf{D}_{\mathrm{tran}}$ and $\mathbf{D}_{\mathrm{rot}}$ are diagonal matrices of translational and rotational resistive-force coefficients of the body, and $\mathbf{S}_{\mathrm{b}}$ is the skew-symmetric matrix signifying the cross-products. Further, $\mathbf{Z}_{\mathrm{t}_1}$ and $\mathbf{Z}_{\mathrm{t}_2}$ are the resistance matrices of the first and second tails and are given by

$$\mathbf{Z}_{\mathrm{t}_i} = \int_0^{l_{\mathrm{t}_i}} \begin{pmatrix} \mathbf{R}_i\mathbf{C}_i\mathbf{R}_i^{\mathrm{T}} & -\mathbf{R}_i\mathbf{C}_i\mathbf{R}_i^{\mathrm{T}}\mathbf{S}_{\mathrm{t}_i} \\ \mathbf{S}_{\mathrm{t}_i}\mathbf{R}_i\mathbf{C}_i\mathbf{R}_i^{\mathrm{T}} & -\mathbf{S}_{\mathrm{t}_i}\mathbf{R}_i\mathbf{C}_i\mathbf{R}_i^{\mathrm{T}}\mathbf{S}_{\mathrm{t}_i} \end{pmatrix} \mathrm{d}l_{t_i}, \tag{2}$$

where l_{t_i} is the length of the ith tail. Further, $\mathbf{S}_{\mathrm{t}_i}$ is the skew-symmetric matrix satisfying the cross-products, $\mathbf{C}_i$ and $\mathbf{R}_i$ are the diagonal matrix of the local resistive force coefficients, and the rotation matrix from local Frenet-Serret coordinate frames to the inertial frame of reference of the microrobot along the ith tail, respectively [23], and given by

$$\mathbf{C}_i = \begin{pmatrix} C_{\mathrm{t}_i} & 0 & 0 \\ 0 & C_{\mathrm{n}_i} & 0 \\ 0 & 0 & C_{\mathrm{b}_i} \end{pmatrix} \text{ and } \mathbf{R}_i = [\mathbf{t}_i \ \ \mathbf{n}_i \ \ \mathbf{b}_i], \tag{3}$$

where $C_{\mathrm{t}_i} = -2\pi\mu/(\ln(\frac{l_{\mathrm{t}_i}}{r_{\mathrm{t}_i}}) - 0.807)$ is the ith tangential local force coefficient [24], μ is the dynamic viscosity of the medium and r_{t_i} is the ith tail radius. The ith normal and binormal local force coefficients are $C_{\mathrm{n}_i} = C_{\mathrm{b}_i} = -4\pi\mu/(\ln(\frac{l_{\mathrm{t}_i}}{r_{\mathrm{t}_i}}) + 0.193)$. Further, $\mathbf{t}_i$, $\mathbf{n}_i$, and $\mathbf{b}_i$ are the following local tangent, normal, and binormal vectors of the ith flexible tail, for i=1,2, respectively:

$$\mathbf{t}_i = \frac{\mathrm{d}\mathbf{p}_i/\mathrm{d}x}{\| \mathrm{d}\mathbf{p}_i/\mathrm{d}x \|}, \mathbf{n}_i = \frac{\mathrm{d}\mathbf{t}_i/\mathrm{d}x}{\| \mathrm{d}\mathbf{t}_i/\mathrm{d}x \|}, \mathbf{b}_i = \mathbf{t}_i \times \mathbf{n}_i, \tag{4}$$

where $\mathbf{p}_i = [x \ \ \varphi_i \ \ z]^{\mathrm{T}}$ is the local deformation vector and φ_i is the ith tail deformation. The local time-dependent Frenet-Serret frames ($\mathbf{t}_i$, $\mathbf{n}_i$, and $\mathbf{b}_i$) in (4) are determined by solving the following structural deformation equation of the two-tailed microrobot:

$$\begin{aligned} E_iI_i\frac{\partial^4\varphi_i}{\partial x^4} = f_y + \left(J_i + \frac{m_iE_iI_i}{k_iA_iG_i}\right)\frac{\partial^4\varphi_i}{\partial t^2\partial x^2} \\ + \frac{J_i}{k_iA_iG_i}\frac{\partial^2 f_y}{\partial t^2} - \frac{E_iI_i}{k_iA_iG_i}\frac{\partial^2 f_y}{\partial x^2} \\ - m_i\frac{\partial^2\varphi_i}{\partial t^2} - \frac{J_im_i}{k_iA_iG_i}\frac{\partial^4\varphi_i}{\partial t^4}, \end{aligned} \tag{5}$$

where E_i and I_i are the modulus of elasticity and second moment of area of the ith tail, respectively. f_y is the lateral hydrodynamic force acting on the tails. Further, J_i, m_i, and k_i are the moment of inertia per unit length, mass, and shape correction coefficient [25], respectively. A_i, and G_i are the cross-section area and shear modulus of the ith tail, respectively. The local hydrodynamic forces acting on the flexible tail are given by

$$[f_x \ \ f_y \ \ f_z]^{\mathrm{T}} = \begin{bmatrix} \mathbf{R}_i\mathbf{C}_i\mathbf{R}_i^{\mathrm{T}} & -\mathbf{R}_i\mathbf{C}_i\mathbf{R}_i^{\mathrm{T}}\mathbf{S}_{\mathrm{t}_i} \end{bmatrix} \begin{bmatrix} \mathbf{U} \\ \mathbf{\Omega} \end{bmatrix}, \tag{6}$$

where $\mathbf{U}$ and $\mathbf{\Omega}$ are the linear and angular velocities of the microrobot, respectively. Now the equation of motion of the microrobot based on the force-free swimming condition is

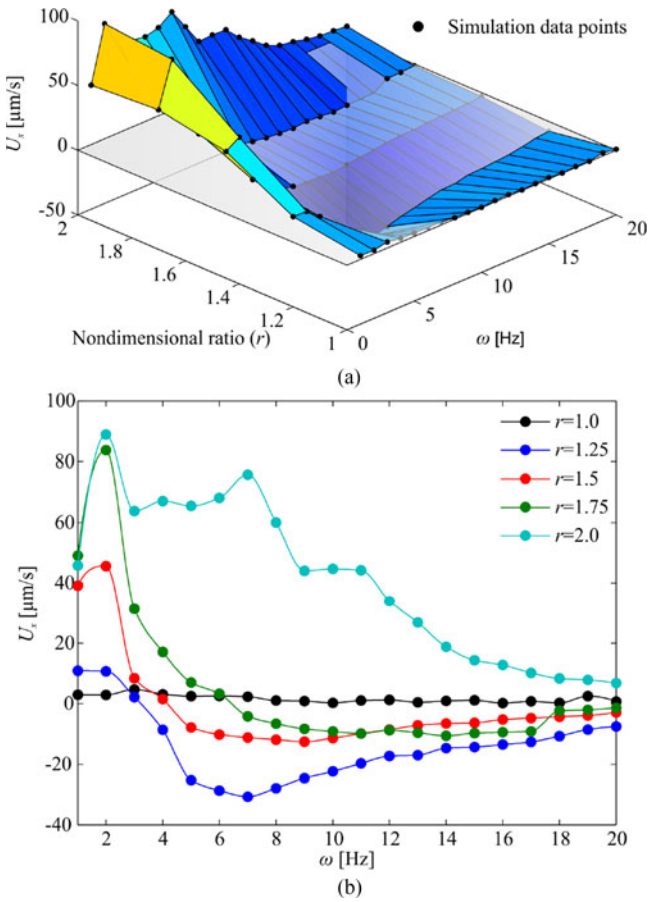

Fig. 2. Forward speed (U_x) of the two-tailed microrobot is calculated versus the tail length ratio (r) and the actuation frequency ω. The speed is calculated using (7) for a 215-μm-long first tail, and minor and major diameter of 25 μm and 80 μm, respectively. Length of the second tail is increased to achieve tail length ratio $r = \frac{l_1}{l_2}$ of 1, 1.25, 1.5, 1.75, and 2. The modulus of elasticity (E) of the tails is 0.58 GPa. (a) The transparent plane intersects with the three-dimensional surface at the reversal frequencies at which the microrobot achieves negligible net displacement. The black circles indicate the calculated speeds of the microrobot. (b) The frequency responses indicate that the long tail (for $r = 1.25$, 1.5, and 1.75) provides greater propulsive force at relatively low actuation frequencies, and as the frequency increases the short tail generates greater propulsive force and thus the microrobot swims along the opposite direction. For $r = 2$, the short tail does not provide enough propulsive force to change the direction of the microrobot and thus results in several inflection points.

given by

$$\begin{pmatrix} \mathbf{U} \\ \mathbf{\Omega} \end{pmatrix} = -\mathbf{Z}_{\mathrm{r}}^{-1} \begin{pmatrix} V\left(\mathbf{m}\cdot\nabla\right)\left(\mathbf{R}_{\mathrm{r}}\mathbf{B}\right) \\ V\mathbf{m}\times\left(\mathbf{R}_{\mathrm{r}}\mathbf{B}\right) \end{pmatrix}, \tag{7}$$

where V and $\mathbf{R}_{\mathrm{r}}$ are the volume of the magnetic particles embedded into the polymer matrix of the head and a rotation matrix between the frame of reference of the microrobot and the laboratory frame of reference.

In order to study the influence of the two tails on the overall behaviour of the microrobot, we define the tail length ratio $r = \frac{l_1}{l_2}$. (1)–(7) are solved for distinct tail length ratios of 1 to 2 with a step of 0.125. At each tail length ratio, we allow the periodic magnetic field to vary with frequency ω throughout a frequency range of 1 Hz to 20 Hz. Fig. 2 shows the forward velocity (U_x) of two-tailed microrobots. (7) also provides the velocity components along lateral directions. The forward velocity is calculated for a 215-μm-long short tail and the length of the second tail is set based on the mentioned tail length ratios. The minor and major diameters of the head are 25 μm and 80 μm, respectively. The radius of the tails is 7 μm and the viscosity of the medium is 0.95 Pa.s. The modulus of elasticity of the tails is measured using depth sensing indentation as 0.58 GPa [21]. Unlike one-tailed microrobots which have a unique maximum velocity, two-tailed microrobots ($r = 1.25$, 1.5, and 1.75) have two exterma with opposite signs, as shown in Fig. 2(a). The implication of having two tails is that zero swimming speed can be achieved at reversal frequencies (ω_{r}) that depend on the tail length ratio. These reversal frequencies exist between the cut-off frequencies of each tail. The calculated velocities in Fig. 2(b) shows that the long tail provides greater propulsive force than the short tail at relatively low actuation frequency. Therefore, microrobots (with $1.25 \leq r \leq 1.75$) have two cut-off frequencies for each tail, and a unique reversal frequency between its cut-off frequencies. For instance, microrobots with tail length ratio of 1.25, 1.5, and 1.75 reverse their swimming direction at actuation frequency of 3.2 Hz, 4.2 Hz, and 6.4 Hz, respectively. However, microrobots with tail length ratio of 2 do not reverse their motion regardless to the actuation frequency [see Fig. 2(b)]. The propulsive force of the short tail does not enable the microrobot to reverse its direction and thus results in several exterma along the velocity profile owing to its dependence on the actuation frequency. We fabricate microrobots and characterize their response to validate our theoretical prediction.

III. Characterization of the Reversal Frequencies of Two-Tailed Microrobots

Two-tailed microrobots are fabricated with tail length ratios of approximately 1.25, 1.5, and 1.75. These ratios are devised based on the calculated speeds (see Fig. 2) of the microrobots at actuation frequency range of 1 Hz to 20 Hz. The microrobots are contained inside a deep chamber filled with glycerin with viscosity of 0.95 Pas, and are allowed to swim below the glycerin-air interface. Four electromagnetic coils with orthogonal configuration are used to provide periodic magnetic field and achieve flagellar propulsion. Each coil (with wire thickness of 0.7 mm and 3200 turns) has length of 80 mm and inner- and outer-diameter of 20 mm and 40 mm, respectively. The microrobots are adjusted within the common center of the electromagnetic coils before each characterization experiment. At this position the magnetic field and magnetic field gradient are measured to be 18 mT and 5 T/m, respectively. The difference between the drag and magnetic forces along the direction of propulsion is on the order of $\mathcal{O}(10^{-4})$ μN and thus propulsion of the microrobots is solely due to its beating flexible tails.

Frequency response of the two-tailed microrobots is characterized for each tail length ratio. The forward speed (U_x) is calculated at each actuation frequency to determine the reversal frequency of the microrobots. Fig. 3(a) shows the frequency response of microrobots with $r \simeq 1.5$ and $r \simeq 1.75$. We observe that microrobots with $r \simeq 1.25$ have reversal

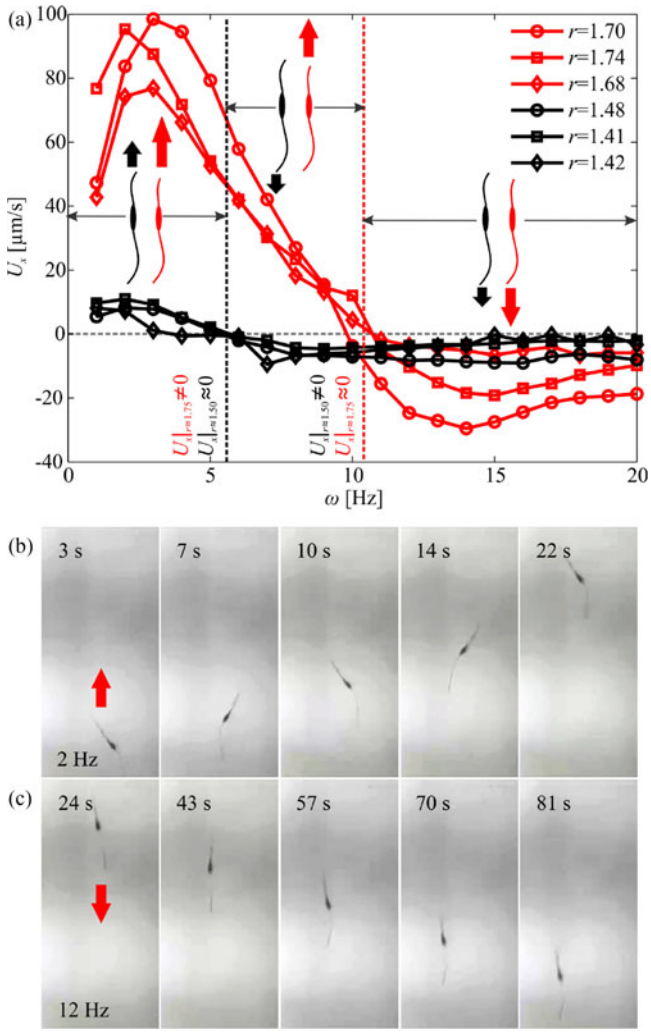

Fig. 3. Frequency responses of two groups of two-tailed microrobots indicate their different response to a common magnetic field. (a) Periodic magnetic field at $\omega \simeq 6$ Hz (black dashed vertical line) enables microrobots with tail ratio of 1.75 to swim while keeping microrobots with tail length ratio of 1.5 fixed. At frequency of 10 Hz, microrobot with tail length ratio of 1.5 swims, while microrobot with tail length ratio 1.75 is fixed. (b) Microrobot ($r \simeq 1.75$) swims at speed of $U_x = 60$ μm/s and $U_y = 2.31$ μm/s, at $\omega = 2$ Hz. (c) The microrobot swims along the opposite direction at speed of $U_x = 20$ μm/s and $U_y = 2.55$ μm/s, at $\omega = 12$ Hz. *Please refer to the accompanying video.*

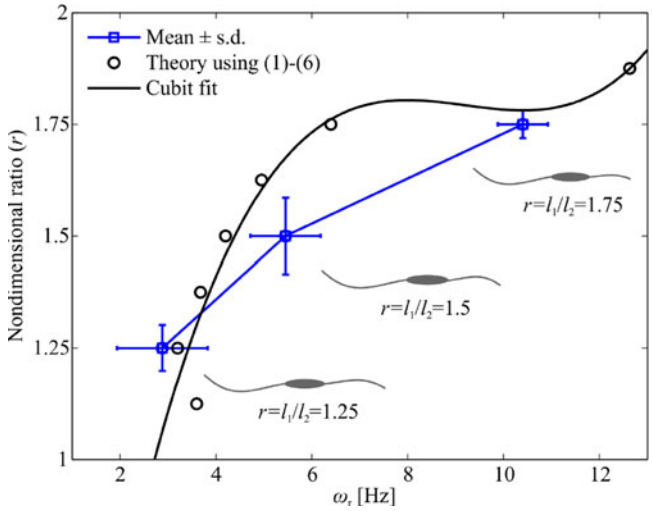

Fig. 4. Calculated and measured reversal frequencies (ω_r) of the two-tailed microrobots for ratio (r) of 1.25, 1.5, and 1.75. The reversal frequencies are calculated using (7) for a 215-μm-long first tail, and minor and major diameter of 25 μm and 80 μm, respectively. Length of the second tail is increased to achieve tail length ratios $r = \frac{l_1}{l_2}$ of 1, 1.25, 1.5, 1.75, and 2. The averages and standard deviations (s.d.) of the reversal frequencies and tail length ratios are calculated using 6 samples from each group.

frequency of 2.8 ± 0.9 Hz, and the tail-length ratio is measured to be 1.24 ± 0.11. Therefore, microrobots with $r \simeq 1.25$ achieve zero displacement under the influence of periodic magnetic field at $\omega = 2.8$ Hz. At this reversal frequency, the short and long tails impart almost equal and opposite propulsive forces to the fluid, and hence negligible net displacement is achieved. In addition, the microrobot swims along opposite directions below and above $\omega_r = 2.8$ Hz. The reversal frequency of microrobots with $r = 1.5$ is measured to be 5.4 ± 0.7 Hz, whereas their ratio is 1.48 ± 0.08. Fig. 3 shows the response of three microrobots with $r = 1.48$, $r = 1.41$, and $r = 1.42$. In these ratios, microrobots achieve negligible displacement under the influence of periodic magnetic field of approximately 5.4 Hz.

The reversal frequency increases with the tail length ratio. For $r = 1.75$, the reversal frequency increases to 10.4 ± 0.5 Hz and the tail length ratio is measured to be 1.71 ± 0.09. At this ratio, two-tailed microrobot achieves negligible displacement under the influence of periodic magnetic field at $\omega \simeq 10$ Hz. Fig. 3(b) shows the response of a microrobot with $r = 1.75$. At $\omega \simeq 2$ Hz, the microrobot swims at an average speed of $U_x = 60$ μm/s and lateral speed of $U_y = 2.31$ μm/s. We observe that its speed decreases with the increasing actuation frequency and reverses its direction above $\omega = 10$ Hz. At $\omega = 12$ Hz, the microrobot swims along the opposite direction at an average speed of $U_x = 20$ μm/s and lateral speed of $U_y = 2.55$ μm/s, as shown in Fig. 3(c). *Please refer to the accompanying video.*

The relation between the reversal frequency of the two-tailed microrobots and their tail length ratio is shown in Fig. 4. We find a qualitative agreement between the predicted reversal frequencies using our RFT-based hydrodynamic model and experimental results for tail length ratio of 1.25, 1.5, and 1.75. The black curve is fitted to the simulation results obtained by solving (7) for a range of tail length ratio of 1.125 to 1.875 with a step of 0.125. Average velocities and standard deviations for three ratios ($r = 1.25$, 1.5, and 1.75) are measured using six samples for each tail length ratio. The theoretical model presented in (1)–(7) predicts reversal frequencies of 3.2 Hz, 4.2 Hz, 6.4 Hz whereas the measured reversal frequencies are 2.8 ± 0.9 Hz, 5.4 ± 0.7 Hz, and 10.4 ± 0.5 Hz for $r = 1.25$, 1.5, and 1.75, respectively. The differences between the theoretical predictions and measurements are attributed to errors in some of the parameters that enter the model. These errors influence our theoretical predictions as RFT theory is based on time-dependent velocity and force prediction that necessitates accurate extraction of resistive-force coefficients. Our experimental results and theoretical prediction show that the reversal frequency increases with the tail length ratio. Therefore, adding multiple microrobots with different reversal frequency enables independent maneuvering using a common driving magnetic field.

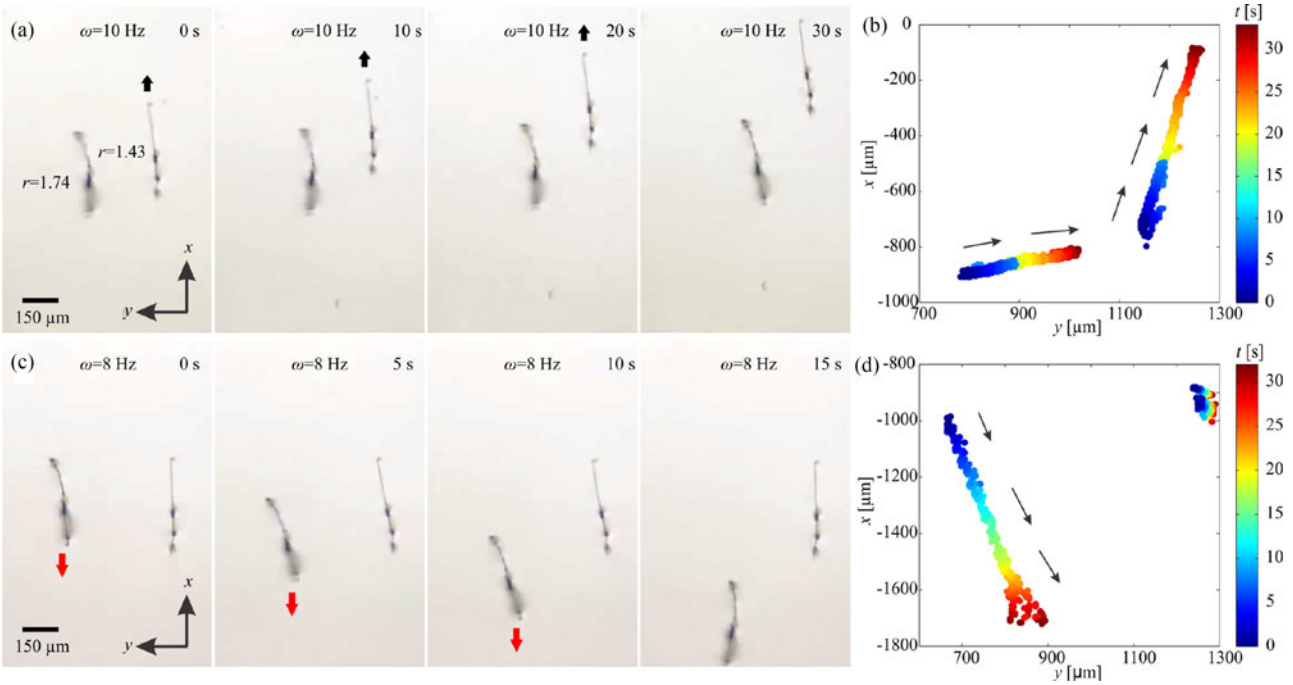

Fig. 5. Independent flagellar propulsion of 2 two-tailed microrobots is achieved using a common periodic magnetic field. The first (left) and second (right) microrobots have tail length ratios of 1.74 and 1.43, respectively. (a) Under the influence of periodic magnetic field at frequency of 10 Hz, the first robot achieves negligible displacement, whereas the second microrobot swims at an average speed of 15.92 μm/s. (b) The trajectories shows that microrobot with tail length ratio of 1.74 drifts sideways and does not move forward. (c) At $\omega = 8$ Hz, the first microrobot swims at an average speed of 44.11 μm/s, while the second microrobot achieves negligible displacement. (d) The trajectories taken by the microrobots indicate that microrobot with tail length ratio of 1.43 does not swim or drift at its reversal frequency. The black arrows indicate the direction of the microrobots *Please refer to the accompanying video.*

IV. Independent Control of Two-Tailed Microrobots

We demonstrate open-loop and closed-loop independent control by applying a common magnetic field to microrobots with different tail length ratios.

A. Open-Loop Independent Actuation

Fig. 5(a) shows the response of two microrobots with tail length ratios of 1.43 and 1.73. A microrobot with 260-μm-long and 150-μm-long first and second tails is placed next to another microrobot with 290-μm-long and 202-μm-long first and second tails, respectively. The two microrobots are separated with approximately one body length to decrease their influence on each other. However, the flagellar beating of the ultra-thin flexible tails of the microrobots induces frequency dependant flow-field, and as a consequence, the other microrobot drifts based on the induced field [26]. First, we show the ability to move one microrobot only and then reverse this action to demonstrate selective actuation and flagellar propulsion of one of the two-tailed microrobots. Periodic magnetic field at $\omega = 10$ Hz is applied. This frequency is close to the reversal frequency of microrobots with $r = 1.73$, and as a consequence, the microrobot with $r = 1.73$ (left) achieves negligible net displacement along its long axis, while the other microrobot (right) with $r = 1.43$ swims at an average speed of 15.92 μm/s and its induced flow-field is responsible for the drift of the other microrobot at speed of $U_y = 7.5$ μm/s. The trajectories taken by the two microrobots are shown in Fig. 5(b). These trajectories indicate that the microrobot with tail length ratio of 1.73 does not achieve flagellar swim but drifts sideways.

Now we reverse this action by applying periodic magnetic field at $\omega = 8$ Hz, as shown in Fig. 5(c). We observe that the microrobot with $r = 1.43$ achieves negligible displacement, while the other microrobot with $r = 1.73$ swims at an average speed of 44.11 μm/s and moves along its lateral direction at speed of 7.1 μm/s. Fig. 5(d) shows the trajectories taken by the microrobots and indicates that microrobot with $r = 1.43$ achieves negligible displacement and does not drift, while the microrobot with $r = 1.73$ drifts while achieving flagellar propulsion. This behaviour is observed more at relatively low actuation frequencies [see Fig. 5(b)] and has less influence at relatively high actuation frequencies.

It is also possible to actuate the two-tailed microrobots simultaneously along one direction based on the frequency response in Fig. 3. Fig. 6(a) demonstrates this response using periodic magnetic field at $\omega = 3$ Hz. At this frequency the microrobot with $r = 1.43$ swims at an average speed of 61.34 μm/s, whereas the other microrobot swims at 23.66 μm/s along the same direction [see Fig. 6(b)]. The frequency response of the microrobots also suggests that motion reversal can be achieved above the reversal frequencies of both microrobots. Again this behaviour is demonstrated in Fig. 6(c). We apply periodic magnetic field at $\omega = 16$ Hz. This common magnetic field enables the microrobots with $r = 1.43$ and $r = 1.73$ to swim along the

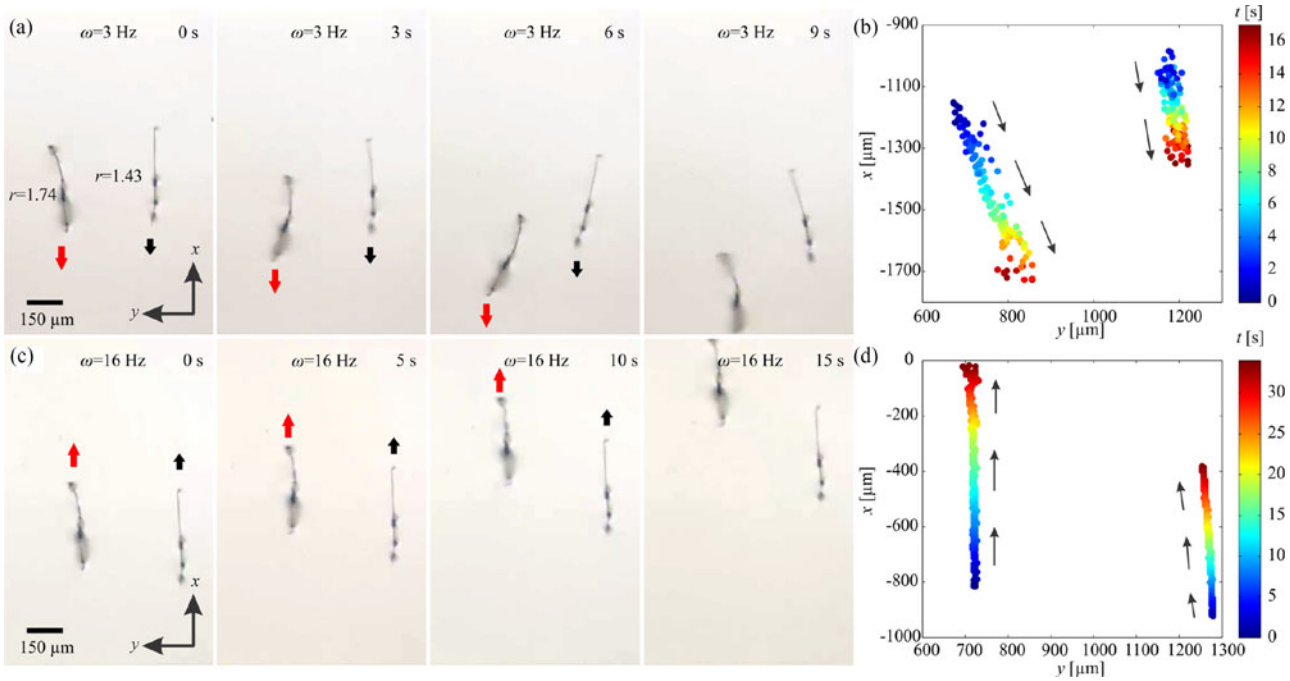

Fig. 6. Independent flagellar propulsion of 2 two-tailed microrobots is achieved using a common periodic magnetic field. The first (left) and second (right) microrobots have tail length ratios of 1.74 and 1.43, respectively. (a) Under the influence of periodic magnetic field at frequency of 3 Hz, the first and second microrobot swim along same direction at an average speed of 61.34 μm/s and 23.66 μm/s, respectively. (b) Trajectories of the microrobot indicate a slight sideways motion during flagellar propulsion. (c) At $\omega = 16$ Hz, the first and second microrobot swim along same direction at an average speed of 50.43 μm/s and 28.69 μm/s, respectively. (d) The trajectories taken by the microrobots indicate negligible motion along the lateral direction of the microrobots. The black arrows indicate the direction of motion of the microrobots. *Please refer to the accompanying video.*

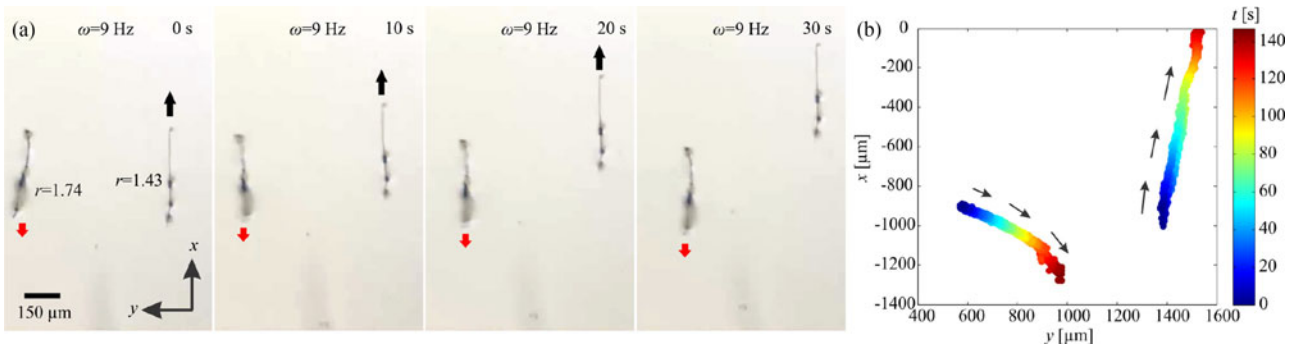

Fig. 7. Independent flagellar propulsion of 2 two-tailed microrobots is achieved using a common periodic magnetic field. (a) The first (left) and second (right) microrobots have tail length ratios of 1.74 and 1.43, respectively. The microrobots are controlled to swim along opposite directions. The first and second microrobots swim at average speed of 4 μm/s and 16.34 μm/s under the influence of periodic magnetic field at frequency of 9 Hz. (b) The trajectories indicate that microrobot with $r = 1.74$ drifts sideways while swimming along opposite direction to microrobot with $r = 1.43$. The black arrows indicate the direction of motion of the microrobots. *Please refer to the accompanying video.*

opposite directions together at average speeds of 50.43 μm/s and 28.69 μm/s [see Fig. 6(d)], respectively. *Please refer to the accompanying video.*

The frequency response of the two-tailed microrobots also indicates actuation frequencies that enable the two microrobots to swim along opposite directions. Fig. 3 shows that within actuation frequencies of 5 Hz and 10 Hz, microrobots with $r = 1.5$ and $r = 1.75$ swim along opposite directions using a common magnetic field. This response is demonstrated in Fig. 7(a). We apply periodic magnetic field at $\omega = 9$ Hz and observe that the two microrobots swim along opposite directions. The microrobot with $r = 1.43$ swims at an average speed of 4 μm/s, whereas the other microrobot with $r = 1.73$ swims along the opposite direction at 16.34 μm/s and drifts sideways, as shown in Fig. 7(b). Although our theoretical model does not account for interactions between microrobots, our experimental results on single and two microrobots indicate that lateral motion is caused by the induced flow-field of the flexible tails of the microrobots. Fig. 3 shows representative flagellar propulsion of single microrobot with negligible lateral velocity component owing to absence of interaction with another microrobot, whereas Figs. 5–7 indicate hydrodynamic interactions caused by the induced flow-field of two microrobots [26]. This effect can be mitigated by implementing closed-loop motion control to correct the direction of propulsion. *Please refer to the accompanying video.*

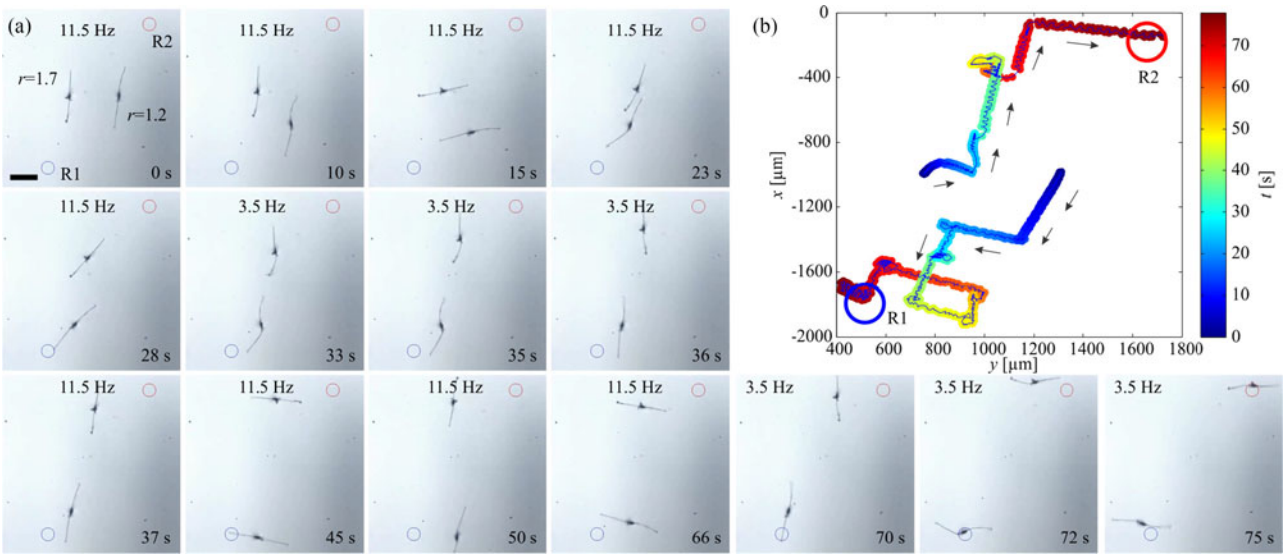

Fig. 8. Closed-loop control of 2 two-tailed microrobots with $r = 1.2$ and $r = 1.7$ is achieved towards two reference positions. (a) Microrobot with $r = 1.2$ is controlled to swim towards reference position R1 at $\omega = 11.5$ Hz (reversal frequency of microrobot with $r = 1.7$). Microrobot with $r = 1.7$ is controlled to swim towards reference position R2 at $\omega = 3.5$ Hz (reversal frequency of microrobot with $r = 1.7$). The reference positions are indicated using the blue and red circles. Scale bar is 350 μm. (b) The trajectories of the microrobots indicate that the microrobots are positioned within the vicinity of the two reference position with steady-state errors of 175 μm and 72 μm for microrobots with $r = 1.2$ and $r = 1.7$, respectively. *Please refer to the accompanying video.*

B. Independent Motion Control of Microrobots

We implement independent motion control of 2 two-tailed microrobots by teleoperation with an Exterme 3D pro Joystick (963290-0403, logitech, Newark, USA). Our control strategy capitalizes mainly on the reversal frequencies of each microrobot, and is implemented as follows: (1) We determine the reversal frequencies (based on Fig. 4) of the first and second microrobots (ω_{r_1} and ω_{r_2}). (2) Two reference positions (R1 and R2) are selected in any arbitrary location for each microrobot. (3) Position errors between R1 and the center of mass of the spheroidal head of microrobot ① and R2 and center of mass of microrobot ② are measured. (4) Uniform magnetic fields pointing towards R1 are applied based on the calculated position error [27]. (5) A periodic component is applied at ω_{r_2} and switched off when microrobot ① reaches at R1. (6) Uniform magnetic fields are applied towards R2. (7) Periodic component is applied at ω_{r_1} and switched off when microrobot ② reaches at R2.

The mentioned control strategy is based on actuating one microrobot with the reversal frequency of the other, and vice versa. Therefore, microrobot ② achieves negligible displacement while microrobot ① is swimming towards R1 at ω_{r_2}, and vice versa. Fig. 8 shows a representative control trial of 2 two-tailed microrobots with tail length ratios of 1.2 and 1.7. The reversal frequency of the microrobot with $r = 1.2$ is 3.5 Hz, whereas the reversal frequency of the microrobot with $r = 1.7$ is 11.5 Hz. At the time interval, $0 < t < 33$ seconds, uniform magnetic field is applied and oriented towards R1 with periodic component at $\omega = 11.5$ Hz. In this interval, microrobot with $r = 1.7$ achieves negligible displacement and orients itself with the dynamic magnetic field [see Fig. 8(a)]. At time, $t = 33$ seconds, the frequency of the periodic component is switched to 3.5 Hz to allow the microrobot with $r = 1.7$ to swim towards R2. Once the two microrobots are separated with approximately one body length, the control system switches the frequency to adjust each microrobot within the vicinity of its reference position. Fig. 8(b) shows the trajectories taken by the microrobots in this representative trial and indicates that the steady-state errors of microrobots with $r = 1.2$ and $r = 1.7$ are 175 μm and 72 μm, respectively. The average positioning errors of the two-tailed microrobots within the vicinity of R1 and R2 are 110.1 ± 91.8 μm and 146.9 ± 105.9 μm, respectively. *Please refer to the accompanying video.*

V. Conclusions and Future Work

We demonstrate independent locomotion of two-tailed microrobots with different tail length ratio under the influence of a common driving magnetic field. The microrobots are modeled using RFT to predict the influence of the tail length ratio and actuation frequency on their propulsion. Our model predicts distinct parametric spaces (tail length ratio and actuation frequencies) that enable selective actuation and motion differentiation of microrobots. We also find qualitative and quantitative agreement between our theoretical prediction and experimental results. Our experimental results shows that the reversal frequencies of the microrobots are 2.8 ± 0.9 Hz, 5.4 ± 0.7 Hz, and 10.4 ± 0.5 Hz for tail length ratios of 1.24 ± 0.11, 1.48 ± 0.08, and 1.71 ± 0.09, respectively, whereas our model predicts reversal frequencies of 3.2 Hz, 4.2 Hz, and 6.4 Hz for tail length ratios of 1.25, 1.5, and 1.75, respectively. We also implement selective actuation of microrobots, simultaneous flagellar propulsion along one direction, and simultaneous propulsion along opposite directions. In addition, independent motion control of two-tailed microrobots towards different reference positions is demonstrated based on their characterized reversal frequencies.

As part of future studies, we will implement independent motion control of multiple (more than two) two-tailed microrobots

towards several reference positions. This level of control is necessary to enable multiple microrobots to accomplish complex tasks that require execution of different tasks simultaneously. Our current RFT-based hydrodynamic model predicts the behaviour of a single microrobot for a range of tail length ratio and actuation frequencies. The model will be modified to predict the interactions between adjacent microrobots and the flow-field generated by two-tailed microrobots will be measured using particle image velocimetry for single and multiple two-tailed microrobots. This modification is necessary to study the influence of microrobots on each other during actuation and motion control of multiple microrobots.

REFERENCES

[1] E. M. Purcell, "Life at low Reynolds number," *Amer. J. Phys.*, vol. 45, no. 1, pp. 3–11, Jun. 1977.

[2] H. Gadêlha., "On the optimal shape of magnetic swimmers," *Reg. Chaotic Dyn.*, vol. 18, no. 1–2, pp. 75–84, Jan. 2013.

[3] C. H. Wiggins and R. E. Goldstein, "Flexive and propulsive dynamics of elastica at low Reynolds number," *Phys. Rev. Lett.*, vol. 80, no. 17, pp. 3879–3882, Apr. 1998.

[4] J. J. Abbott *et al.*, "How should microrobots swim?" *Int. J. Robot. Res.*, vol. 28, no. 11–12, pp. 1434–1447, Nov. 2009.

[5] E. L. Tony, S. Yu, and A. E. Hosoi, "Experimental investigations of elastic tail propulsion at low Reynolds number," *Phys. Fluids*, vol. 18, Sep. 2006, Art. no. 091701.

[6] H.-W. Huang, Q. Chao, M. S. Sakar, and B. J. Nelson, "Optimization of tail geometry for the propulsion of soft microrobots," *IEEE Robot. Autom. Lett.*, vol. 2, no. 2, pp. 727–732, Jan. 2017.

[7] W. Gao, S. Sattayasamitsathit, K. M. Manesh, D. Weihs, and J. Wang, "Magnetically powered flexible metal nanowire motors," *J. Amer. Chem. Soc.*, vol. 132, no. 41, pp. 14403–14405, Sep. 2010.

[8] T. Xu, C. Vong, B. Wang, L. Liu, X. Wu, and L. Zhang, "Rotating soft-tail millimeter-scaled swimmers with superhydrophilic or superhydrophobic surfaces," in *Proc. IEEE Int. Conf. Biomed. Robot. Biomechatronics*, Singapore, Jul. 2016, pp. 502–507.

[9] I. S. M. Khalil *et al.*, "Sperm-shaped magnetic microrobots: Fabrication using electrospinning, modeling, and characterization," in *Proc. IEEE Int. Conf. Robot. Autom.*, Stockholm, Sweden, May 2016, pp. 1939–1944.

[10] O. S. Pak, W. Gao, J. Wang, and E. Lauga, "High-speed propulsion of flexible nanowire motors: Theory and experiments," *Soft Matter*, vol. 7, pp. 8169–8181, Jul. 2011.

[11] B. Jang *et al.*, "Undulatory locomotion of magnetic multilink nanoswimmers," *Nano Lett.*, vol. 15, no. 7, pp. 4829–4833, Jun. 2015.

[12] H.-W. Huang, Q. Chao, M. S. Sakar, and B. J. Nelson, "Optimization of tail geometry for the propulsion of soft microrobots," *IEEE Robot. Autom. Lett.*, vol. 2, no. 2, pp. 727–732, Apr. 2017.

[13] B. R. Donald, C. G. Levey, and I. Paprotny, "Planar microassembly by parallel actuation of MEMS microrobots," *J. Microelectromech. Syst.*, vol. 17, no. 4, pp. 789–808, Aug. 2008.

[14] S. Floyd, E. Diller, C. Pawashe, and M. Sitti, "Control methodologies for a heterogeneous group of untethered magnetic micro-robots," *Int. J. Robot. Res.*, vol. 30, pp. 1553–1565, Mar. 2011.

[15] E. Diller, J. Giltinan, and M. Sitti, "Independent control of multiple magnetic microrobots in three dimensions," *Int. J. Robot. Res.*, vol. 32, no. 5, pp. 614–631, May 2013.

[16] E. Diller, J. Giltinan, P. Jena, and M. Sitti, "Three dimensional independent control of multiple magnetic microrobots," in *Proc. IEEE Int. Conf. Robot. Autom.*, Karlsruhe, Germany, May 2013, pp. 2576–2581.

[17] B. Kratochvil, D. Frutiger, K. Vollmers, and B. Nelson, "Visual servoing and characterization of resonant magnetic actuators for decoupled locomotion of multiple untethered mobile microrobots," in *Proc. IEEE Int. Conf. Robot. Autom.*, Kobe, Japan, May 2009, pp. 1010–1015.

[18] A. W. Mahoney, N. D. Nelson, K. E. Peyer, B. J. Nelson, and J. J. Abbott, "Behavior of rotating magnetic microrobots above the step-out frequency with application to control of multi-microrobot systems," *Appl. Phys. Lett.*, vol. 104, Apr. 2014, Art. no. 144101.

[19] D. Wong, J. Wang, E. Steager, and V. Kumar, "Control of multiple magnetic micro robots," in *Proc. Int. Des. Eng. Techn. Conf. Comput. Inform. Eng. Conf.*, Boston, MA, USA, Aug. 2015, pp. 1–8.

[20] D. Cappelleri, D. Efthymiou, A. Goswami, N. Vitoroulis, and M. Zavlanos, "Towards mobile microrobot swarms for additive micromanufacturing," *Int. J. Adv. Robotic Syst.*, vol. 11, no. 9, pp. 1–14, Sep. 2014.

[21] I. S. M. Khalil *et al.*, "Swimming back and forth using planar flagellar propulsion at low Reynolds numbers," *Adv. Sci.*, 2017, Art. no. 1700461. [Online]. Available: https://doi.org/10.1002/advs.201700461

[22] I. S. M. Khalil, A. F. Tabak, A. Klingner, and M. Sitti, "Magnetic propulsion of robotic sperms at low-Reynolds number," *Appl. Phys. Lett.*, vol. 109, Jul. 2016, Art. no. 033701.

[23] A. J. Hanson and H. Ma, "Quaternion frame approach to streamline visualization," *IEEE Trans. Visual. Comput. Graph.*, vol. 1, no. 2, pp. 164–174, Jun. 1995.

[24] C. Brennen and H. Winet, "Fluid mechanics of propulsion by cilia and flagella," *Annu. Rev. Fluid Mech.*, vol. 9, pp. 339–398, Jan. 1977.

[25] T. Kaneko, "On Timoshenko's correction for shear in vibrating beams," *J. Phys. D, Appl. Phys.*, vol. 8, no. 16, pp. 1927–1936, Nov. 1975.

[26] J. Happel and H. Brenner, *Low Reynolds Number Hydrodynamics With Special Applications to Particulate Media*. Englewood Cliffs, NJ, USA: Prentice-Hall, 1965.

[27] I. S. M. Khalil, H. C. Dijkslag, L. Abelmann, and S. Misra, "MagnetoSperm: A microrobot that navigates using weak magnetic fields," *Appl. Phys. Lett.*, vol. 104, Jun. 2014, Art. no. 223701.